Materials Advances

ROYAL SOCIETY OF CHEMISTRY

PAPER

View Article Online
View Journal | View Issue

Cite this: *Mater. Adv.*, 2020, 1, 463

Nanocrystalline microstructure in Sm^{3+} and Gd^{3+} doped K_2O–MgO–Al_2O_3–SiO_2–F glass-ceramic sealant (SOFC)

Mrinmoy Garai, *[ab] C. Hari Venkateswara Rao[ac] and Basudeb Karmakar[b]

Received 7th April 2020,
Accepted 11th May 2020

DOI: 10.1039/d0ma00179a

rsc.li/materials-advances

In order to demonstrate the effects of Sm^{3+} and Gd^{3+} ions on the crystalline microstructures of the magnesium-boro-alumino-silicate (MBAS) system, the K_2O–MgO–B_2O_3–Al_2O_3–SiO_2–F glass doped with 0–5 mol% Sm_2O_3 and Gd_2O_3 were synthesized by melt-quenching (1550 °C). The addition of Sm^{3+} and Gd^{3+} content was found to increase the density (2.74–2.91 g cm^{-3}) of the base glass. By controlled heat-treatment at 950 °C, the MBAS glasses were converted into opaque glass-ceramics with crystalline phases (XRD), containing fluorophlogopite mica [$KMg_3(AlSi_3O_{10})F_2$], norbergite [$Mg_2SiO_4{\cdot}MgF_2$] and enstatite [$MgSiO_3$]. The FESEM study revealed the development of rock-like and plate-like crystallite particles (average size 2–4 μm) randomly dispersed in the heat-treated MBAS microstructure, which on the addition of Sm^{3+} and Gd^{3+} ions is restructured into nanocrystalline (size = ~50–400 nm) morphology. The substantial change in the microstructure influenced the corresponding density and thermal expansion properties. The coefficient of thermal expansion for MBAS was estimated to be 10.47(±0.10) × 10^{-6} K^{-1} (50–800 °C), which increased to 11.11–11.29 × 10^{-6} K^{-1} when doped with Sm^{3+} and Gd^{3+}. Such large thermal expansion makes the Sm_2O_3- and Gd_2O_3-doped K_2O–MgO–B_2O_3–Al_2O_3–SiO_2–F glasses suitable for high temperature sealing applications (like SOFC).

Introduction

Fluorophlogopite mica-based glass-ceramics are technologically important materials because of their well-grained microstructure, resulting in a wide range of thermal expansion value suitable for high temperature sealing applications.[1–3] K_2O–MgO–B_2O_3–Al_2O_3–SiO_2–F is a type of magnesium-boro-alumino-silicate (MBAS) system that can be easily crystallized into mica glass-ceramics containing fluorophlogopite [$KMg_3(AlSi_3O_{10})F_2$] phase.[3,4] For this, the most studied technique is the controlled *in situ* crystallization of glass over a temperature 800 °C.[4] In addition to the flexibility to develop an improved fine-grained microstructure with desired thermal properties, these glass-ceramics exhibit consistent reproducibility of properties due to the homogeneity of the as-cast melt glass.[4–6] They typically contain a finite quantity of crystalline ceramic phase produced by the controlled nucleation of highly viscous glass forming melts.[5]

Mica glass-ceramics with dense nanocrystalline-grained microstructure and improved thermal properties are interesting materials for high temperature sealing applications such as solid oxide fuel cells (SOFCs).[7] This is typically due to their compatible thermal expansion with other components used (*viz.* metal electrode, solid electrolyte, interconnect material, *etc.*) in SOFC cell.[6,7] Moreover, they possess layered crystalline structure that can avert the generation and growth of micro-crack during thermal recycling operation performed at high temperature.[6–8] However, the large thermal shock resistivity for those mica glass-ceramics arises due to the wide thermal expansion value.[9–11] Moreover, the wide thermal expansion in the K_2O–MgO–B_2O_3–Al_2O_3–SiO_2–F glasses is obtained due to the layered structure of the mica crystals, which permit structural relaxation along the planes of the flat structural network.[5,10] In general, the thermal properties of the mica glass-ceramic body are affected by the particle size, amount of precipitated mica crystals and their strength.[12] In the production of glass-ceramics, two major factors, namely (i) nucleating agents, and (ii) temperature and time of the heat-treatment influence the size and number of the crystals.[4,5] In magnesium-boro-alumino-silicate based glass-ceramic, the tuning of crystallization has been studied with the doping of nucleating agent such as rare-earth (RE) ions having high ionic field strength.[9,10] Compared to the mono- and di-valent modifier ions, the trivalent RE ions (*viz.*, Nd^{3+}, Sm^{3+}, and Gd^{3+}) play different structural roles both over short and intermediate-range in the alumino-silicate glass.[9–11] During the process of crystallization the RE ions (RE^{3+}) tend to 'cluster' that makes a minority of oxygen ions (O^{2-}) involved in the RE–O–RE linkages, and isolated from the aluminosilicate glass.[10,13] Nicoleau *et al.*[13]

[a] *Office of the Additional Director General, Aeronautical Quality Assurance (AQA), Koraput, India. E-mail: mrinmoygarai@yahoo.in*
[b] *Glass Science and Technology Section, CSIR-Central Glass & Ceramic Research Institute (CGCRI), Kolkata, India*
[c] *Department of Mechanical Engineering, Osmania University, Hyderabad, India*

studied the impact of rare-earth silicate crystallization on the borosilicate glass structural configuration and argued that the crystallization leads to the reorganization of the cation distribution around the rare-earth elements. Due to low solubility, the lanthanides lead to crystalline phases in the Si–O–B based glass during cooling.[13,14] This means that the RE ions influence the crystallization behavior, which is essential for preparing glass-ceramics with desired thermal properties required for high-temperature sealing applications (SOFC).[10–13] Salinigopal *et al.*[14] studied the effects of Nd_2O_3 and Gd_2O_3 on the $BaO–Al_2O_3–B_2O_3–SiO_2$ glass and observed that the coefficient of thermal expansion for glass-ceramics lie within the range 12.32–12.81 $\times$ 10^{-6} $^{\circ}C^{-1}$, which is suitable for the solid oxide fuel cell (SOFC) applications.

In this study, based on the previous experiences,[9–11] $40SiO_2–12MgO–16Al_2O_3–10B_2O_3–10K_2O–12MgF_2$ (mol%) glass doped with Sm_2O_3/Gd_2O_3 (5 mol%) was considered as the starting composition in order to achieve a fluorophlogopite (phase) dominated glass-ceramics possessing a high thermal expansion value ($>11 \times 10^{-6}$ K^{-1} at 50–800 °C) suitable for high temperature sealant applications. In this regard, the role of Sm_2O_3 or Gd_2O_3 to improve the glass-ceramic morphology and thermal expansion was also investigated.

Experimental

Three different glasses of (i) base composition (mol%) $40SiO_2–12MgO–16Al_2O_3–10B_2O_3–10K_2O–12MgF_2$ (G-1) and doped (5 mol%) with (ii) Sm_2O_3 (G-2) and (iii) Gd_2O_3 (G-3) were synthesized *via* a conventional melt-quench technique using highly pure reagent grade fine chemicals. Most of the chemicals used were in the form of oxides, hydroxides and carbonates as precursor materials: SiO_2 (Quartz Powder, LobaChemie, Mumbai, India), $Mg(OH)_2$ (97%, LobaChemie, Mumbai, India), $Al(OH)_3$ (97%, LobaChemie, Mumbai, India), H_3BO_3 (99.5%, LobaChemie, Mumbai, India), K_2CO_3 (98%, LobaChemie, Mumbai, India), MgF_2 (99.9%, LobaChemie, Mumbai, India), Sm_2O_3 (99.99%, Indian Rare Earths Ltd, Udyogamandal, India) and Gd_2O_3 (99.99%, Indian Rare Earths Ltd, Udyogamandal, India). Homogeneously mixed batches were allowed to melt at ~1550 °C (2 h) using an electric furnace (Kanthal), followed by stirring for 0.5 min with a silica glass rod in an open platinum (Pt) crucible. Molten glasses were then allowed to cast into a pre-heated carbon plate in open-air atmosphere. The as-synthesized glasses were then heat-treated at ~950 °C (2 h) for controlled crystallization.

The density (d) of the investigated glass and glass-ceramic bulk samples was determined (with an accuracy of ±0.7%) by the Archimedes principle using distilled water as the immersion liquid (density = 1 g cc^{-1}) in a digital balance (MettlerToledo), which enables weighing the bulk solid in air (W_{air}) as well as in the solvent (W_{water}):

$$d = [W_{air}/(W_{air} - W_{water})]d_{water}$$

The crystallinity of the studied samples (glass and corresponding glass-ceramics) was checked *via* powder X-ray diffraction (XRD). All the patterns were recorded on a XPERTPRO MPD diffractometer (PANalytical, Netherlands) operating with Ni-filtered Cu Kα (λ = 1.5406 Å) radiation, irradiated at 40 kV and 40 mA. The crystalline phases were analyzed in the 2θ range of 5–70° with a step size of 0.05° at room temperature.

The microstructural morphology of the studied glass-ceramics (heat-treated at 950 °C/2 h) were examined *via* field emission scanning electron microscopy (FESEM model S430i, LEO, CEA, USA) using polished glass-ceramic samples (chemically etched by immersion in 5 vol% aqueous HF solution for 5 min).

In order to investigate the thermal properties, the coefficient of thermal expansion (CTE) of the studied glass-ceramics were evaluated using a cylinder-shaped sample with a length of ~25 mm and diameter of ~6 mm using a horizontal dilatometer, NETZSCH DIL 402 PC (NETZSCH-Gerätebau GmbH, Germany) at a heating rate of 5 °C min^{-1} under ±1% accuracy after calibration with a standard Al_2O_3 cylinder.

Results and discussion

The melt-quenched monoliths of $40SiO_2–12MgO–16Al_2O_3–10B_2O_3–10K_2O–12MgF_2–Sm_2O_3/Gd_2O_3$ (0–5 mol%) composition were opaque in nature. Base glass G-1 contained no rare-earth composition; it possessed density value 2.74 ± 0.02 g cm^{-3}. On adding Sm_2O_3 and Gd_2O_3 in the G-1 glass, the density increased to 2.85 ± 0.02 and 2.91 ± 0.02 g cm^{-3}, respectively.[10] The as-synthesized glasses were heat-treated at 950 °C for 2 h over, which they were converted into the glass-ceramics. The crystalline nature of the glasses and corresponding glass-ceramics were accounted from the XRD pattern taken in 5–70° (2θ). It is evident from Fig. 1 that the broad hump appearing at (2θ) 15–35° for all the glasses signifies their amorphous nature.[10,12] On heating over 950 °C, those glasses converted into glass-ceramic signifying their crystalline pattern (XRD), as exhibited

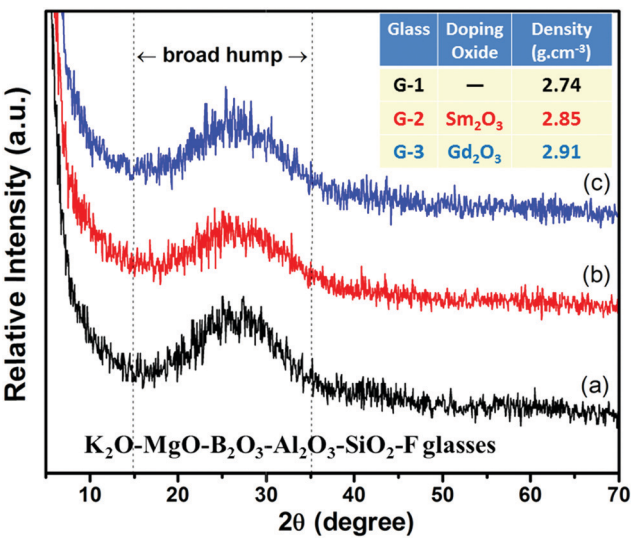

Fig. 1 XRD pattern of the as-synthesized glasses (a) G-1 (b) G-2 and (c) G-3 showing the appearance of a broad hump in the range at (2θ) 15–35° signifying their amorphous characteristics (inset shows the density values of glasses).

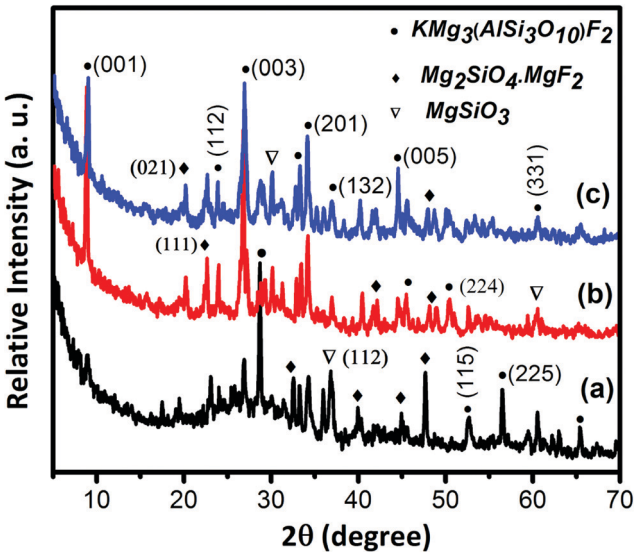

Fig. 2 XRD pattern of the heat-treated glass-ceramics (a) G-1 (b) G-2 and (c) G-3 showing their multi-crystalline nature with crystalline phases fluorophlogopite mica [$KMg_3(AlSi_3O_{10})F_2$], norbergite [$Mg_2SiO_4{\cdot}MgF_2$] and enstatite [$MgSiO_3$].

in Fig. 2. The crystalline peaks shown in Fig. 2 at the (2θ) positions of 8.92, 23.82, 26.92, 33.43, 34.18, 37.03, 44.54, 46.05, 50.42, 52.79, 56.48, 60.57 and 65.26°, corresponding to the (001), (112), (003), (200), (201), (132), (005), (222), (224), (115), (225), (331) and (007) planes are developed due to the formation of the phase fluorophlogopite mica, $KMg_3AlSi_3O_{10}F_2$ (molecular weight = 421, monoclinic end-centered system, JCPDS-PDF number 10-0494 & 71-1542; lattice parameter a = 5.299, b = 9.188, c = 10.13).[3,5] All the peaks with corresponding planes are summarized in Table 1.

The characteristic peaks appearing at (2θ) 19.93, 22.67, 32.42, 39.90, 41.75, 45.40 and 48.94° diffracted from the (021), (111), (131), (210), (004), (142) and (151) crystalline planes, correspond to the formation of magnesium fluoride silicate, 'Norbergite' ($Mg_2SiO_4{\cdot}MgF_2$), molecular weight = 203, JCPDS file number 71-2401 (orthorhombic, primitive system; lattice parameter a = 4.710, b = 10.27, c = 8.747). Norbergite is formed in all the glass-ceramics; however, the development of fluorophlogopite mica is supported by rare-earth ions.[10,13,14] A different crystalline phase enriched by the Mg and Si contents, magnesium silicate, 'enstatite' ($MgSiO_3$), molecular weight = 100.39, was also found to appear with peaks (2θ) 30.20, 36.78 and 60.45° due to the crystalline planes (321), (112) and (650); JCPDS file number 83-2057 (orthorhombic, primitive system; lattice parameter a = 18.21, b = 8.813, c = 5.179).[15] During the heat-treatment, Mg^{2+} and F^- ions tend to form MgF_2 precipitates at ~600–650 °C.[16] The tiny particles of MgF_2 then mix with magnesium silicates to form the additive compound *i.e.*, norbergite crystallites.[10,16] In the base glass-ceramic, the XRD pattern manifests the appearance of norbergite and enstatite phases predominantly. The trivalent ions Sm^{3+} or Gd^{3+} strongly support the heterogeneous phase separation in the SiO_2–MgO–Al_2O_3–B_2O_3–K_2O–MgF_2 composition.[10,14] Due to the large ionic field strength (charge/radius) and small critical nuclei, they tend to form 'clusters' during initial heating, and hence are isolated from the silicate glass network (Si–O–Si).[10,11] Thus, the maximum XRD peaks corresponding to the fluorophlogopite phase are observed in the case of G-2 (*i.e.*, Sm_2O_3 content) and G-3 (*i.e.*, Gd_2O_3 content) glass-ceramics.[13,14] Under the same heat-treatment, the slight shift of the diffraction peaks in G-2 and G-3 (Fig. 2) is associated with the crystallite size and high concentration of the fluorophlogopite phase.[15,17]

Mica belongs to the monoclinic system with the co-existence of several types of atoms, where the volume fraction, crystallinity and grain size of the crystalline phase is controlled by the heat-treatment as well as the doping agents.[5,17] In the present report, the controlled nucleation in the SiO_2–MgO–Al_2O_3–B_2O_3–K_2O–MgF_2 glass is performed under two selected parameters: (i) heat-treatment at 950 °C for 2 h and (ii) the addition of 5 mol% Sm_2O_3 and Gd_2O_3. Thus, it is of interest to compare the microstructures of the crystallized glasses of same composition with different RE ions. Volume crystallization with a rather fine morphology was observed for all the glass-ceramics studied under same heat-treatment.[18–20] The examples of the FESEM micrographs (taken using etched G-1 to G-3 specimens) are given in Fig. 3. The XRD analysis of these samples indicated that the base glass-ceramic microstructure predominantly contained norbergite and enstatite constituents, and the rare-earth doped samples (Sm_2O_3 and Gd_2O_3) largely comprised fluorophlogopite mica particles.[10] As seen from Fig. 3a, the G-1 glass-ceramic microstructure is composed of rock-like and plate-like crystallite particles (average size 2 to 4 μm), which are randomly dispersed throughout the matrix. In a closer look it seems that the plenty of rock-shaped (100–500 nm sized) particles are in-homogeneously positioned to fill the gaps amongst the plate-shape crystallites of dimension 1–4 μm. The bulk density of the G-1 glass-ceramic was calculated as 2.77 ± 0.02 g cm^{-3}. In the presence of Sm_2O_3 (*i.e.*, Sm^{3+}), the glass-ceramic structure is largely changed into the nanocrystalline morphology,[10–14] where 50–200 nm sized spherical droplets such as crystallite particles are homogeneously distributed to

Table 1 XRD peaks and corresponding planes of different crystalline phases developed in studied K_2O–MgO–B_2O_3–Al_2O_3–SiO_2–F glass-ceramics heat-treated at 950 °C for 2 h

Peak position (2θ) (degree)	Corresponding planes	Crystalline phase	JCPDS file
8.92, 23.82, 26.92, 33.43, 34.18, 37.03, 44.54, 46.05, 50.42, 52.79, 56.48, 60.57, 65.26	(001), (112), (003), (200), (201), (132), (005), (222), (224), (115), (225), (331), (007)	Fluorophlogopite mica [$KMg_3AlSi_3O_{10}F_2$]	10-0494 and 71-1542
19.93, 22.67, 32.42, 39.90, 41.75, 45.40, 48.94	(021), (111), (131), (210), (004), (142), (151)	Norbergite ($Mg_2SiO_4{\cdot}MgF_2$)	71-2401
30.20, 36.78, 60.45	(321), (112), (650)	Enstatite ($MgSiO_3$)	83-2057

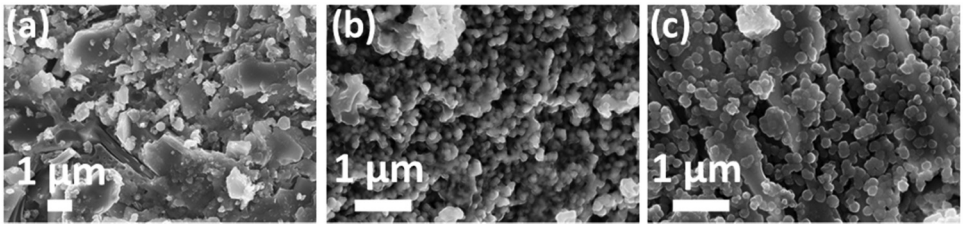

Fig. 3 FESEM photomicrograph of G-1 (a), G-2 (b) and G-3 (c) glass-ceramics heat-treated at 950 °C, showing the restructure of plate-like crystallites into spherical granule-like crystallites in attendance of with the RE content (Sm_2O_3 and Gd_2O_3).

form a fine-grained microstructure (Fig. 3b). Such a compact morphology is ascribed for its high density value (3.02 ± 0.02 g cm^{-3}).[6,20] During the heat-treatment at 950 °C, the nucleating agents such as Sm^{3+} or Gd^{3+} ions can either support the heterogeneous phase separation or these can cause the accumulation in a specific microphase or nanophase of the phase separated glass.[3,10] Those trivalent ions Sm^{3+} or Gd^{3+} having large ionic field strength (charge/radius) and smaller critical nuclei tend to form 'cluster', which makes a minority of oxide ions involved in the Sm–O–Sm or Gd–O–Gd linkages, and hence isolated from the silicate glass network (Si–O–Si).[10,11,13] When Gd_2O_3 (*i.e.*, Gd^{3+}) is present in the base composition G-1, the spherical granules are agglomerated in the surrounds of Gd^{3+} to form 'cluster'. The clusters then shaped into bigger spherical crystals mostly of size, 200–400 nm (Fig. 3c).[10,14] From samarium (Sm) to gadolinium (Gd) the ionic radii decreases and hence the ionic field strength increases by virtue of ''lanthanide contraction''. Therefore, it can be guessed that Gd^{3+} have occupied the interstitial places in the glass network governed by Si–O–Si/B–O–B/Si–O–B and their increase in field strength as well as atomic weight have made the glass-ceramic network more compact, resulting in an increase in the molecular weight without increasing the volume.[10] Thus, the maximum density is estimated for G-3 as 3.06 ± 0.02 g cm^{-3}.[6,20]

The dilatometry of the heat-treated samples (*i.e.*, glass-ceramics) was carried out in order to investigate the thermal expansion-sealant (SOFC) behavior.[21,22] A plot of the CTE of the glass-ceramics between 400 °C and 800 °C is presented in Fig. 4. Linear increase in CTE up to 800 °C was obtained for all the studied glass-ceramics; however, the linear trend is quite different for the Sm_2O_3- and Gd_2O_3-doped samples. For the G-1 glass-ceramic, the CTE at 50–500 °C was 8.00(±0.08) × 10^{-6} K^{-1} and increased to 8.20, 9.37 and 10.54 × 10^{-6} K^{-1} at 50–600, 50–700 and 50–800 °C, respectively. For G-2, where 5 mol% Sm_2O_3 was added, the CTE was evaluated as 8.44(±0.08) and 8.56(±0.09) × 10^{-6} K^{-1} at 50–500 °C and 50–600 °C, respectively. The obtained CTE values are summarized in Table 2. For fluorophlogopite mica-based glass-ceramics, the CTE strongly depends on the size, shape of crystallite particles as well as crystalline fraction in the microstructure.[23,24] The dopant ions Sm^{3+} or Gd^{3+} have tendency to participate in the overall bonding of the MBAS glass to tailor the thermal expansion since their structural roles in the Si–O–Si matrix are related to their size and coordination number.[9–11] Nanocrystalline morphology advocates structural relaxation in the G-2 glass-ceramic in comparison

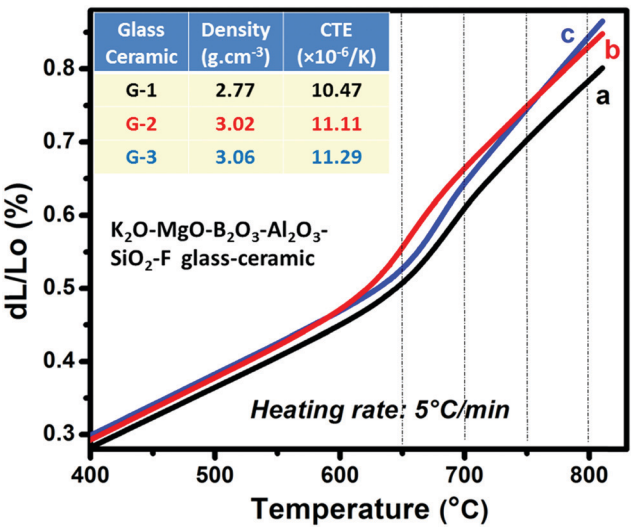

Fig. 4 Variation of thermal expansion as a function of temperature for fluorophlogopite glass-ceramics (heat-treated at 950 °C) with and without doped rare-earth ion content (inset shows the density of glass-ceramics and their CTE value at the SOFC operation temperature).

Table 2 Variation of the thermal expansion value (CTE) of different K_2O–MgO–B_2O_3–Al_2O_3–SiO_2–F glass-ceramics heat-treated at 950 °C for 2 h

Sample identity	Coefficient of thermal expansion (× 10^{-6} K^{-1})			
	50–500 °C	50–600 °C	50–700 °C	50–800 °C
G-1	8.00(±0.08)	8.20(±0.08)	9.37(±0.09)	10.47(±0.10)
G-2	8.44(±0.08)	8.56(±0.09)	10.22(±0.10)	11.11(±0.11)
G-3	8.56(±0.09)	8.53(±0.09)	9.89(±0.10)	11.29(±0.11)

to the G-1 system.[10,13,23] At 50–700 and 50–800 °C, large CTE values were thus estimated for the G-2 sample with the values being 10.22(±0.10) and 11.11(±0.11) × 10^{-6} K^{-1}, respectively. Gd^{3+} having a smaller size gets surrounded by the $[AlO_4]^-$ tetrahedra during heat-treatment. In the present composition, 5 mol% Gd_2O_3 was present in the $40SiO_2$–$12MgO$–$16Al_2O_3$–$10B_2O_3$–$10K_2O$–$12MgF_2$ system and the microstructure of that became less homogeneous.[10,11] As is evident from Fig. 3c, the dimension of the spherical crystallite particles increased, whereas the compactness of the morphology decreased. Because of the combining effects, the CTE value of G-3 is comparatively larger at 50–800 °C (Table 2).[9,10]

For intermediate temperature (700–800 °C) solid oxide fuel cell (SOFC) designs, the glass sealant must have thermal expansion

characteristics that do not contribute to the creation of thermal stress between a variety of ceramic and metallic materials used in the SOFC stack; must be thermochemically compatible with the other materials; must be stable at operational temperatures (700–800 °C) of SOFCs. These all requirements are however controlled by the CTE value.[25–29] Thus, a linear thermal expansion up to 800 °C as well as large CTE value at that temperature are prime requisites for SOFC sealant.[28] The large CTE ($>11 \times 10^{-6}$ K^{-1}) at 50–800 °C as observed for the samples G-2 and G-3 (Table 2), is well-matched with the SOFC components like electrode (Ni/Fe), solid electrolyte (YSZ), interconnect (Crofer-22APU) *etc.* in the operating temperature ~700–800 °C.[23,24] Hence, Sm_2O_3 and Gd_2O_3 doped SiO_2–MgO–Al_2O_3–B_2O_3–K_2O–MgF_2 glasses can act as a potential SOFC sealant material.[13,30]

Conclusions

This report highlights the effect of the addition of samarium (Sm^{3+}) and gadolinium (Gd^{3+}) on the nucleation behavior, alteration of microstructure, physical and thermal properties of low alkali containing magnesium-boro-alumino-silicate (MBAS) glass. 0–5 mol% Sm_2O_3 and Gd_2O_3 doped K_2O–MgO–B_2O_3–Al_2O_3–SiO_2–F glasses were synthesized by melt-quenching at 1550 °C. The major conclusions are summarized below:

• Base glass G-1 (no rare-earth composition) possessed density value of 2.74 ± 0.02 g cm^{-3}, which after the addition of Sm^{3+} and Gd^{3+} increased to 2.85–2.91 g cm^{-3}.

• The MBAS glasses, by controlled heat-treatment at 950 °C (2 h), were converted into multi-crystalline grass-ceramics with predominantly crystalline phase (XRD) containing fluoro-phlogopite mica [$KMg_3(AlSi_3O_{10})F_2$], norbergite [$Mg_2SiO_4 \cdot MgF_2$] and enstatite [$MgSiO_3$].

• Field emission scanning electron microscopy revealed the development of rock-like and plate-like crystallites (average size ~2–4 μm) randomly dispersed in the base glass-ceramic matrix. In the presence of Sm^{3+} and Gd^{3+}, the microstructure restructured into nanocrystalline morphology packed by droplet-like crystallite particles (size ~50–400 nm).

• The significant variation in microstructure is ascribed to the corresponding density and thermal expansion value. The coefficient of thermal expansion (CTE) for the base glass-ceramic was estimated to be $10.47(\pm 0.10) \times 10^{-6}$ K^{-1} at 50–800 °C that increased to $11.11–11.29 \times 10^{-6}$ K^{-1} at 50–800 °C for glass-ceramics containing Sm^{3+} and Gd^{3+}. Such large thermal expansion makes the Sm_2O_3- and Gd_2O_3-doped K_2O–MgO–B_2O_3–Al_2O_3–SiO_2–F glasses applicable for high temperature sealing application (like SOFC).

Conflicts of interest

There are no conflicts to declare.

Acknowledgements

MG thankfully acknowledges CSIR for the financial support under the CSIR-NMITLI project TLP 0005. The authors are very much thankful to Dr K. Muraleedharan, Director and Dr Ranjan Sen, Head, Glass Division and Dr R. N. Basu, Head, Fuel Cell and Battery Division of CSIR-CGCRI, Kolkata for their encouragement and support to carry out this work. They thankfully acknowledge the technical supports provided by the XRD and SEM Sections of CSIR-CGCRI.

References

1 W. Holand, V. Rheinberger and M. Schweiger, *Adv. Eng. Mater.*, 2001, **3**, 768–774.
2 G. H. Beall, *Int. J. Appl. Glass Sci.*, 2014, **5**, 93–103.
3 M. Garai, N. Sasmal, A. R. Molla, S. P. Singh, A. Tarafder and B. Karmakar, *J. Mater. Sci.*, 2014, **49**, 1612–1623.
4 J. Deubener and W. Höland, *Front. Mater.*, 2017, **4**, 14.
5 W. Wolfgang and C. Rüssel, *CrystEngComm*, 2015, **17**(45), 8671–8675.
6 M. Garai and B. Karmakar, *Front. Mater.*, 2020, **7**, 57.
7 Y. S. Chou, J. W. Stevenson and P. Singh, *J. Power Sources*, 2005, **152**, 168–174.
8 H. Liu, X. Du, Z. Yu, D. Tang and T. Zhang, *RSC Adv.*, 2016, **6**, 17151.
9 N. Sasmal, M. Garai, A. R. Molla, A. Tarafder, S. P. Singh and B. Karmakar, *J. Non-Cryst. Solids*, 2014, **387**, 62–70.
10 M. Garai and B. Karmakar, *J. Alloys Compd.*, 2016, **678**, 360–369.
11 N. Sasmal, M. Garai and B. Karmakar, *J. Asian Ceram. Soc.*, 2016, **4**, 29–38.
12 A. Chen, W. Tan, H. He, G. Li, X. Wu, Q. Tao and J. Zhu, *Phys. Chem. Miner.*, 2019, **46**(3), 259–270.
13 E. Nicoleau, F. Angeli, S. Schuller, T. Charpentier, P. Jollivet and M. Moskura, *J. Non-Cryst. Solids*, 2016, **438**, 37–48.
14 M. S. Salinigopal, N. Gopakumar, P. S. Anjana and O. P. Pandey, *J. Non-Cryst. Solids*, 2020, **535**, 119956.
15 T. Benitez, A. Veber, K. P. Furlan, L. B. Rebouças, D. de Ligny, D. Hotza, A. P. N. de Oliveira and N. Travitzky, *Int. J. Appl. Glass Sci.*, 2020, **11**(1), 155–169.
16 M. Garai, N. Sasmal, A. R. Molla, A. Tarafder and B. Karmakar, *J. Mater. Sci. Technol.*, 2015, **31**, 110–119.
17 T. Behraznia, A. S. Alzahrani, M. Rashwan, A. J. Bushby and R. G. Hill, *J. Eur. Ceram. Soc.*, 2020, **40**(3), 887–892.
18 H. Yu, W. Li, W. G. Zhu and H. B. Wu, *Glass Phys. Chem.*, 2019, **45**(6), 555–564.
19 M. Eilaghi, M. Montazerian and B. E. Yekta, *Trans. Indian Ceram. Soc.*, 2016, **75**(1), 1–6.
20 M. Garai, A. K. Maurya and S. Roy, *MRS Adv.*, 2018, **3**, 3525–3533.
21 V. Kumar, M. Kaur, G. Kaur, S. K. Arya and G. Pickrell, Stacking designs and sealing principles for IT-solid oxide fuel cell, *Intermediate Temperature Solid Oxide Fuel Cells*, Elsevier, 2020, pp. 379–410.
22 S. Ghosh, P. Kundu, A. Das Sharma, R. N. Basu and H. S. Maiti, *J. Eur. Ceram. Soc.*, 2008, **28**, 69–76.
23 M. Garai, N. Sasmal and B. Karmakar, *Indian J. Mater. Sci.*, 2015, **2015**, 638341, DOI: 10.1155/2015/638341.

24 A. A. Reddy, A. Goel, D. U. Tulyaganov, M. Sardo, L. Mafra, M. J. Pascual, V. V. Kharton, E. V. Tsipis, V. A. Kolotygin and J. M. F. Ferreira, *J. Mater. Chem. A*, 2014, **2**(6), 1834–1846.
25 M. Garai, T. S. R. Ch Murthy and B. Karmakar, *Ceram. Int.*, 2018, **44**, 22308–22317.
26 P. Nandi, A. S. Patil, B. Paul, A. Sarkar, M. Goswami and G. P. Kothiyal, *Trans. Indian Ceram. Soc.*, 2012, **71**(4), 235–238.
27 M. Garai, N. Sasmal, A. R. Molla and B. Karmakar, *Solid State Sci.*, 2015, **44**, 10–21.
28 D. A. Krainova, S. T. Zharkinova, N. S. Saetova, A. A. Raskovalov, A. V. Kuz'min, V. A. Eremin, E. A. Sherstobitova, S. V. Pershina, M. V. Dyadenko, X. Zhang and S. Jiang, *Russ. J. Appl. Chem.*, 2017, **90**(8), 1278–1284.
29 X. V. Nguyen, C. T. Chang, G. B. Jung, S. H. Chan, W. T. Lee, S. W. Chang and I. C. Kao, *Int. J. Hydrogen Energy*, 2016, **41**(46), 21812–21819.
30 S. Kurama and G. Saydam, *J. Aust. Ceram. Soc.*, 2017, **53**(2), 293–298.